ECCE AB 21

virtual event

Engineering the Future

13th European Congress on Chemical Engineering
6th European Congress on Applied Biotechnology
20-23 September 2021

The meeting point for researchers across Europe and the world with

- 13 parallel sessions
- Science Slam
- ChemCar Competition
- Virtual exhibition

Find out more and register at ecce-ecab2021.eu

Plenary speakers

Jiří Drahoš,
Senator of the Czech
Parliament Prague/CR

Michael Doherty
University of California
Santa Barbara CA/USA

Luisa Freitas Dos Santos
GlaxoSmithKline plc.
Brentford/UK

Melanie Maas-Brunner
BASF SE
Ludwigshafen/D

Emily Nguyen
Palantir Technologies
New York/USA

Platinum Sponsor

BASF
We create chemistry

Silver Sponsors

Research and Development

Beiersdorf

Organizer

DECHEMA

Supporter

EFCE

ESBES

Received: 4 March 2021 | Revised: 25 May 2021 | Accepted: 11 June 2021

DOI: 10.1002/bit.27861

ARTICLE

BIOTECHNOLOGY AND BIOENGINEERING WILEY

Microfluidic cultivation and analysis of productive biofilms

Phillip Lemke[1] | Ahmed E. Zoheir[1,2] | Kersten S. Rabe[1] | Christof M. Niemeyer[1]

[1]Karlsruhe Institute for Technology (KIT), Institute for Biological Interfaces (IBG 1), Eggenstein-Leopoldshafen, Germany

[2]Department of Genetics and Cytology, National Research Centre (NRC), Cairo, Egypt

Correspondence
Christof M. Niemeyer, Karlsruhe Institute for Technology (KIT), Institute for Biological Interfaces (IBG 1), Hermann-von-Helmholtz-Platz 1, D-76344 Eggenstein-Leopoldshafen, Germany.
Email: niemeyer@kit.edu

Funding information
Helmholtz-Gemeinschaft

Abstract

We here report the application of a machine-based microfluidic biofilm cultivation and analysis platform for studying the performance of biocatalytically active biofilms. By using robotic sampling, we succeeded in spatially resolving the productivity of three microfluidic reactors containing biocatalytically active biofilms that inducibly overexpress recombinant enzymes. *Escherichia coli* biofilms expressing two stereoselective oxidoreductases, the (*R*)-selective alcohol dehydrogenase LbADH and the (*S*)-selective ketoreductase Gre2p, as well as the phenolic acid decarboxylase EsPAD were used. The excellent reproducibility of the cultivation and analysis methods observed for all three systems underlines the usefulness of the new technical platform for the investigation of biofilms. In addition, we demonstrated that the analytical platform also opens up new opportunities to perform in-depth spatially resolved studies on the biomass growth in a reactor channel and its biochemical productivity. Since the platform not only offers the detailed biochemical characterization but also broad capabilities for the morphological study of living biofilms, we believe that our approach can also be performed on many other natural and artificial biofilms to systematically investigate a wide range of process parameters in a highly parallel manner using miniaturized model systems, thus advancing the harnessing of microbial communities for technical purposes.

KEYWORDS
automated biotechnology, biocatalysis, biofilms, microfluidics, stereoselectivity

1 | INTRODUCTION

Biofilms are the most widespread form of microbial life on earth. Biofilms consist of a multitude of different cell types, which are embedded in a complex three-dimensional structure in an extracellular matrix and can therefore colonize even extreme habitats (Flemming et al., 2016). It is becoming increasingly clear that these multicellular communities play an important role for human health and our environment (Hall-Stoodley et al., 2004) and could even serve as tools for the next generation of biotechnological processes (Verstraete, 2015). Since biofilms are resistant to a variety of environmental stresses, their inherited robustness has been exploited primarily for bioremediation. However, due to the ever-growing understanding of these biotic communities, their use as living catalysts for the production of bulk and fine chemicals, as well as for biofuels, biohydrogen and even power generation in microbial fuel cells, is increasingly being expanded (Halan et al., 2012). Due to the general advantages of biofilms, such as increasing the stability of

whole-cell catalysts and performing catalytic reactions under harsh conditions, for instance high temperatures, the development of catalytically active synthetic cellular systems using biofilms and other biofilm-derived materials is currently under investigation (Ahan et al., 2019; Nussbaumer et al., 2017). In addition, biofilms as whole-cell biocatalysts are of particular interest in complex, cofactor-dependent reactions. Due to the metabolic pathways already present in the cells, intracellular regeneration of NADPH can be easily accomplished, eliminating the need to provide additional cofactor-regenerating enzymes (Blank et al., 2008). To use microbial communities as productive biofilms in biotechnological processes as biocatalysts for the production of value-added chemicals, it is essential to bring together engineering and natural sciences to equally consider biological aspects such as biofilm growth, structure, and physiology as well as technical challenges such as reactor configuration and analytics (Muffler & Ulber, 2014). Recent research on productive biofilms generally uses model reactors of mesoscopic size, e.g. to study the continuous production of lactic acid (Cuny et al., 2019), cyclohexanol (Hoschek et al., 2019), or styrene oxide (Schmutzler et al., 2017). However, microfluidic reactors have also been used for this purpose (Karande et al., 2016), for instance, the segmented flow of microdroplets was utilized for the production of perillic acid (Willrodt et al., 2017). We recently reported on machine-assisted cultivation and analysis of biofilms, using a microfluidic platform. It combines readily available microfluidic chips by automated liquid handling not only with conventional analytical instruments for fluorescence detection, microscopy, and chromatography, but also with a specially developed sampling system that enables high spatiotemporal resolution in the analysis of biofilm composition and metabolites (Hansen et al., 2019). We had demonstrated the power of this platform by studying the spatial organization of bacterial cocultures along chemical gradients and by monitoring the productivity of a biofilm in a microfluidic channel.

We report here on the application of the machine-assisted microfluidic cultivation and analysis platform to investigate the performance of biocatalytically active biofilms. For this purpose, a novel sampling method was implemented to flexibly and highly reproducibly investigate selected areas of a microstructured flow channel in which *Escherichia coli* biofilms grow, which express recombinant enzymes. Specifically, we studied *E. coli* biofilms expressing two stereoselective oxidoreductases, the (*R*)-selective alcohol dehydrogenase LbADH and the (*S*)-selective ketoreductase Gre2p, as well as the phenolic acid decarboxylase EsPAD. We demonstrate that the three different biofilms are stably cultivable in the microfluidic platform and that their biocatalytic activity can be investigated by automated sampling in a space- and time-dependent manner. This makes it possible to obtain information about the spatial distribution of the enzyme-expressing cells within the biofilms and to optimize the space-time yields (STY) of the flow-through bioreactors. Therefore, our work illustrates that integrating tools from technical engineering can help advance life sciences to drive the development of sustainable technologies for biochemical production systems.

2 | MATERIALS AND METHODS

All chemicals were purchased from Sigma Aldrich or VWR if not stated otherwise.

2.1 | Bioreactor fabrication, microfluidic setup, and robotic sampler

Microfluidic flow cells with the dimensions of standard microscope slides (76 × 26 mm² DIN ISO 8037-1:2003-05) were used as bioreactors. For decreasing the dead volume, the channel proceeded in a triangular shape to the outlet and inlet, respectively. The effective area of the channel used for biofilm cultivation was 3 mm wide, 1 mm high, and 54 mm long. (Figure S11). This leads to a total volume of about 180 µl. Due to reasons of manufacturing the bioreactor chip consists of two parts, an upper part which is functioning as the lid of the flow cell and the lower part which contains the actual cultivation channel. Both parts were manufactured by replica casting of polydimethylsiloxane (PDMS) (Sylgard 184 (10:1 mix ratio), Dow Corning) in polymethylmethacrylate replication molds. For integration of the bioreactors in the microfluidic system, cannulas (Sterican, B. Braun Melsungen AG) were inserted through holes of the molds to serve as placeholders before curing the liquid PDMS at 70°C for 60 min. The two PDMS parts were bonded together via oxygen plasma treatment using the plasma generator PlasmaFlecto 10 (0.1 mbar, 100% O_2, 300 W, process time: 30 s) (plasma technology GmbH). The basic setup and functionality of the robotic sampling platform was previously described (Hansen et al., 2019). For sampling biofilms grown in the PDMS-bioreactors and to achieve a sampling process without losing parts of the withdrawn sample due to the dead volume of commercially available cannulas, the Luer lock connection was properly sealed with polytetrafluoroethylene-tape (PTFE), thus reducing the dead volume and ensuring a precise sampling of low microliter volumes. The cannula was rinsed automatically with isopropyl alcohol after each sampling process.

2.2 | Cultivation of *E. coli* biofilms

The PDMS bioreactor chips were autoclaved and used for cultivation of *E. coli* BL21 (DE3) which were transformed separately with the plasmid of interest (pET-LbADH-His, pET-Gre2p-His, or pET-EsPAD-His). To this end, the bioreactors were inoculated with an overnight culture (37°C in lysogeny broth (LB) medium supplemented with 100 µg/ml ampicillin). The bioreactors were integrated into the microfluidic system on the robotic deck by connecting them to the silicone tubing (Tygon tubing R3603 (ID = 1.6 mm); Saint-Gobain) using standard cannulas and Luer lock fittings (1/16") (Figure S3a). After a period of 2 h for the initial attachment of the cells to the walls of the bioreactor chips,

the chips were then perfused using syringe pumps with LB-ampicillin-medium for 40 h with the flow rate of interest (6, 12, 24, or 48 µl/min), referred to as the initiation phase. To initialize the protein expression, 1 mM isopropyl-β-D-1-thiogalactopyranoside (IPTG) was supplemented to the medium for 20 h. This phase is referred to as the expression phase.

2.3 | Fluorescence microscopy

To analyze the biofilms via fluorescence microscopy (AxioVert 200M; Carl Zeiss AG) a biofilm expressing mRFP1 was cultivated as described above. Fluorescence images as well as differential interference contrast (DIC) images were taken before and after removal of the biofilm from the reactor. To verify the differentiation between cells and extracellular polymeric substances (EPS), a recombinant expressing eGFP biofilm was grown, flushed out of the reactor by air and the surface-attached biofilm was stained with 0.5% crystal violet (CV; Stiefel et al., 2016). After staining for 25 min at room temperature, the biofilm was washed extensively with water. The reactor was again evacuated and the stained surface attached biofilm left in the reactor was analyzed by fluorescence microscopy using a filter for GFP (Filter Set 44; Carl Zeiss AG) to monitor the fluorescent cells as well as a filter for red fluorescence (Filter Set 43 HE; Carl Zeiss AG) to observe the whole biofilm.

2.4 | High-performance liquid chromatography (HPLC) analysis

To investigate the biocatalytic activity of the biofilms, the bioreactors were perfused via PTFE tubes with LB-ampicillin-IPTG-medium containing 5 mM substrate 5-nitrononane-2,8-dione (NDK) **1** or substrate 4-hydroxycinnamic acid (HCA) **4**. After twice the residence time of the channel, 10 µl samples were taken in case of substrate **1** and 15 µl in case of substrate **4**. Two samples were taken consecutively at each sampling point with the automated sampling robot. Each biofilm was cultivated in duplicates, thus resulting in four samples of each sampling point in total. The samples containing substrate **1** were analyzed as previously described (Peschke, Skoupi, et al., 2017). In brief, the samples were extracted by adding 100 µl ethyl acetate. 70 µl of the organic phase were collected in a microtiter plate, evaporated and the residues analyzed by a chiral HPLC method (90% *n*-heptane, 10% isopropyl alcohol, flow rate: 0.5 ml/min, 10°C, Phenomenex® Lux 3 µm Cellulose-1 150 mm × 2.00 mm). Absorption was detected at 210 nm. In the case of substrate **4**, collected samples were quenched by adding 85 µl 1 mM sulfuric acid. The samples were centrifuged and the supernatant was analyzed by a reverse phase HPLC method (50% acetonitrile, 50% H_2O containing 0.1% trifluoroacetic acid, flow rate: 1.0 ml/min, 35°C, Agilent Technologies® Eclipse XDB-C18 5 µm, 4.6 mm × 150 mm). Absorption was detected at 285 nm (Mittmann, Hu, et al., 2019).

2.5 | Optical density (OD) measurements

For spatially resolved analysis of biomass the biofilms were grown in the flow cell and subsequently the PDMS-bioreactor was cut in five pieces, each of 12.4 mm. The biofilm in each piece was flushed out by pushing air through the channel. The samples were homogenously mixed, and the OD determination was performed by measuring the biofilm samples (1:10 dilution) at 600 nm with a plate reader employing a Take3 Micro-Volume Plate (BioTek Instruments Inc.).

2.6 | Sodium dodecyl sulfate-polyacrylamide gel electrophoresis (SDS-PAGE) analysis

For the subsequent SDS-PAGE the segmented biofilm samples were diluted to OD 0.3 for enzyme-expressing biofilms and OD 0.1 for wild type biofilms, boiled with 4× SDS-PAGE loading buffer (200 mM Tris-Cl, pH 6.8, 400 mM dithiothreitol, 8% SDS, 0.4% bromophenol blue, 40% glycerol) for 10 min at 95°C and loaded on a 12.5% SDS-PAGE gel. The protein containing samples were separated in the gel at 120 V, using PageRuler Prestained Protein Ladder (Thermo Fisher Scientific Inc.) as molecular weight marker. Subsequently, the gel was stained with Coomassie brilliant blue solution for 20 min, destained overnight in water and documented using a FluorChem M imager (ProteinSimple).

2.7 | Western blot analysis

For spatially resolved analysis of the expressed enzyme concentration, the segmented biofilms were analyzed by western blot. To this end, the biofilm samples were diluted (1:900 for EsPAD, 1:600 for LbADH and Gre2p) and additional calibration samples with purified enzyme in a concentration range from 0 to 50 pmol were prepared. For all samples, an SDS-PAGE as described above was performed but instead of the Coomassie brilliant blue staining the gels were transferred onto an Amersham™ Hybond™ polyvinylidene fluoride blotting membrane (Cytiva). The membrane was blocked with 5% skim milk in Tris-buffered saline supplemented with 0.1% Tween-20 (TBST) and incubated with primary anti-His-Tag antibodies (orb68952; Biorbyt Ltd.) in TBST for 2 h. After three successive washing steps with TBST an incubation with secondary antibodies labeled with alkaline phosphatase (AP-112; Columbia Biosciences Corporation) was performed for at least 1 h. The proteins on the membrane were stained using an Alkaline Phosphatase Substrate Kit (Bio-Rad Laboratories Inc.). Images of the membrane were taken with a FluorChem M imager (ProteinSimple) and a greyscale analysis were performed using the open source software Fiji/imageJ (Schindelin et al., 2012).

2.8 | Transmission electron microscopy (TEM)

For the analysis of a productive *E. coli* biofilm by TEM, the biofilm was first grown as described above. After removal of the biofilm

from the reactor by flushing it with air, the sample was diluted 1:10 with PBS buffer (23 mM KH_2PO_4, 77 mM K_2HPO_4, 10 mM NaCl, pH 7.6) and then mixed with the same volume of 2% uranyl acetate. After incubation for 2 min at room temperature, 10 µl of the samples were loaded on a 200-mesh carbon-coated Cu grid (Plano GmbH) and incubated for 2 min. The excess liquid was removed with a filter paper (Whatman™ Grade 1) and the samples were further dried overnight at room temperature. Samples were analyzed using a transmission electron microscope (EM 910 Leo; Carl Zeiss AG) at a voltage of 80 kV.

3 | RESULTS AND DISCUSSION

3.1 | Integrated microfluidic platform for biofilm cultivation and analysis

The technical platform for automated cultivation and analysis of biofilms is shown in Figure 1. A microfluidic chip containing a linear flow channel of 62 mm length, 3 mm width, and 1 mm height was used for the cultivation of biofilms. Microfluidic channels with such dimensions in the millimeter range are known to prevent clogging of the reactor by biofilm growth (Drescher et al., 2013). At the same time, these dimensions ensure the development of a laminar flow in the channel, indicated by a Reynolds number of 0.0718–0.575 (6–48 µl/min). While the previously described flow cells were based on a PDMS microstructure attached to a glass slide (Hansen et al., 2019), here we exchanged them for bioreactors composed entirely of PDMS and adapted the sampling process accordingly to optimize the cultivation platform for productive biofilms. This change was made to exploit the positive influence of the hydrophobic PDMS on the growth of the biofilm compared to growth on glass slides (Alves et al., 2020) and to ensure homogeneous material conditions for biocatalytic conversion. In addition to the simplicity of creating a variety of PDMS structures by replica casting, PDMS generally has certain advantages for the cultivation of cells such as biocompatibility and high gas permeability. Furthermore, the self-sealing property of PDMS after perforation is of particular importance for our platform to ensure non-destructive sampling. However, disadvantages may be that PDMS has a high adsorption capacity for lipophilic small molecules (Toepke & Beebe, 2006). Although this property could be disadvantageous for the biocatalysis investigated here, we observed in preliminary experiments that the biofilms grown in the chip strongly minimize this physical adsorption (Figure S1).

The cultivation system has the feature to directly heat the chip holder as well as the atmosphere in the chamber to allow the control of external factors such as temperature and humidity around the bioreactor chip (Figure S2). A filter with a pore size of 0.2 µm installed at the inlet of the flow cell serves to protect the biofilm from disturbance by small air bubbles and prevents the uncontrollable back-growth of the biofilm into the feed tube, especially at low flow velocities (Figure S3a). The filtration area of 4.9 cm^2 of the commercial filters used in this setup was sufficient to prevent clogging of the filters. We also did not observe any bacterial back-growth in the syringes supplying the nutrient containing LB medium. For the cultivation phase, syringe pumps or pressure-controlled pumps can be used, both of which ensure a fluctuation-free flow of the medium. Both the cultivation of the biofilm and the investigation of its catalytic activity took place directly on the robotic deck, so that the automated sampling could be accomplished without moving the microfluidic system. Figure 1b shows the described setup of the

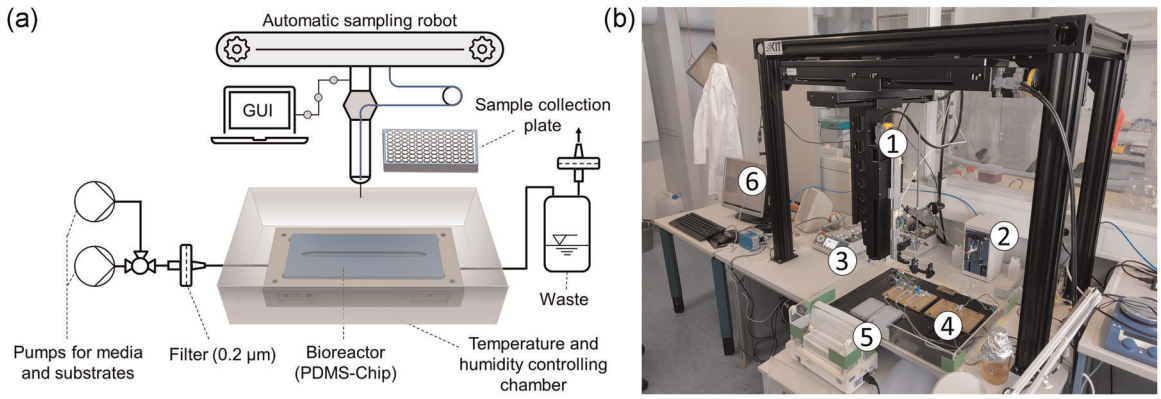

FIGURE 1 Automated biofilm cultivation and sampling platform. Schematic (a) and photographic (b) illustration of the integrated platform for pressure-controlled cultivation and sampling of productive biofilms. The microfluidic bioreactor chip is placed underneath the automated sampling platform which is controlled by the user via a GUI, and enclosed with a chamber around the robotic deck during cultivation to ensure a temperature and humidity-controlled atmosphere. Pumps, valves and filters are part of the microfluidic setup. The photographic overview shows the robotic arm (1) of the sampler. To enable sampling through the PDMS layer of the flow chip, the sample head is equipped with a cannula connected with a high precision pump (2) via PTFE-tubing. For continuous perfusion of the microfluidic system, syringe pumps (3) are used. The bioreactor-chips are mounted on a temperature-controlled chip holder on top of the robotic deck (4) which is enclosed by the incubation chamber (5). The entire system is controlled with a custom-made software (6). Further details on the platform are given in the Figures S2–S4. GUI, graphical user interface; PDMS, polydimethylsiloxane; PTFE, polytetrafluoroethylene [Color figure can be viewed at wileyonlinelibrary.com]

automated biofilm cultivation and sampling platform. We found that additional aeration of the bioreactors was not required for the cultivation of the biofilms, indicating that the oxygen dissolved in the medium as well as the oxygen diffusing through the PDMS was sufficient to ensure the growth of the biofilms. The sampling head has been redesigned to ensure compatibility with commercially available cannulas via standard Luer lock connectors (Figure S3b). In addition, this design allows the mounting of up to two different cannulas, resulting in a more flexible and faster sampling process. To enable precise sampling from the PDMS bioreactors, the sampling head of the robotic sampler is equipped with a cannula, which is connected to a high precision pump to enable withdrawal of defined volumes ranging from 1 to 800 µl. Since it is necessary to monitor the piercing of the PDMS layer for precise sample collection, the sampling cannula is mounted on a pressure-sensitive load cell connected to the robotic arm, which is controlled by a software routine. This made it possible to adapt the automated sampling to changing factors, for example to different material properties such as toughness or elasticity of the flow cell. For a detailed description and additional information on the different units of the platform see Figures S2–S4.

3.2 | Biocatalytic systems

To validate the usefulness of our microfluidic cultivation and analysis platform for the systematic and reproducible analysis of catalytically active biofilms, three enzymatic conversions were selected (Figure 2). The first system is the conversion of the achiral NDK **1** to yield the hydroxyketone intermediates **2a/b** followed by the consecutive reduction to the diol **3a** using an *E. coli* biofilm expressing the (*R*)-selective alcohol dehydrogenase from *Lactobacillus brevis* (LbADH; Figure 2a). Since this system has been previously studied (Hansen et al., 2019; Peschke et al., 2019), it was used to benchmark biofilms that had not been studied before. The second system is the stereoselective conversion of substrate **1** to yield hydroxyketone **2c** by using the (*S*)-selective ketoreductase Gre2p of *Saccharomyces cerevisiae* in *E. coli* biofilm (Figure 2b). This enzyme has a remarkably high stereoselectivity so that only a single product (hydroxyketone **2c**) is formed under regular reaction conditions and no double reduction to the corresponding diol occurs (Peschke, Skoupi, et al., 2017; Skoupi et al., 2015). Furthermore, an *E. coli* biofilm expressing the phenolic acid decarboxylase from *Enterobacter* species (EsPAD) was chosen as the third system (Figure 3c). The EsPAD selectively converts HCA **4** to 4-vinylphenol (VP) **5** (Figure 2c) (Peng et al., 2019). All three enzymes have been immobilized in isolated form in biocatalytic flow reactors in previous work and showed enzymatic activity for at least 40 h, highlighting the stability of these enzymes (Bitterwolf et al., 2019; Mittmann, Gallus, et al., 2019; Mittmann, Hu, et al., 2019; Peschke et al., 2018; Peschke, Rabe, et al., 2017; Peschke, Skoupi, et al., 2017).

To generate the recombinant biofilms, *E. coli* was transformed with the enzyme-encoding plasmids using standard methods and the resulting recombinant bacteria were used for inoculation of the

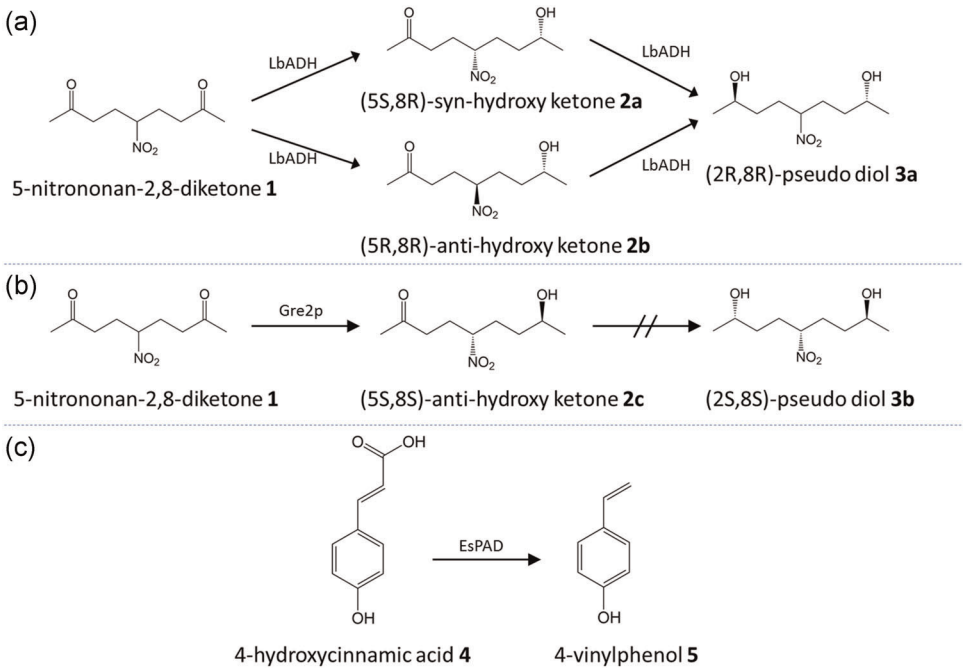

FIGURE 2 Investigated biocatalytic conversions. (a) Stereoselective reduction of the prochiral NDK **1** to yield hydroxy ketone **2a**/**2b** and diol **3a** products by the (*R*)-selective alcohol dehydrogenase LbADH. (b) Reduction of NDK **1** to yield hydroxy ketone **2c** by the (*S*)-selective ketoreductase Gre2p. (c) Conversion of HCA **4** to yield VP **5** by the phenolic acid decarboxylase EsPAD. HCA, 4-hydroxycinnamic acid; NDK, nitro-diketone substrate; VP, 4-vinylphenol

microreactors (see Section 2). In initial experiments, we investigated whether the recombinant biofilms could be cultivated and monitored in the microreactor and whether the transformed plasmids have an influence on the growth of the biofilms and the subsequent protein expression after induction. To this end, the biofilms were grown for 40 h in a continuous flow of LB medium, which in the following is referred to as the initiation phase. To induce the protein expression, the mature biofilms were exposed to a continuous flow of LB medium containing 1 mM IPTG for 20 h. This period is referred to as the expression phase. During the expression phase, the biofilms continue to be supplied with sufficient nutrients to ensure further, continuous growth. However, it is known that after the induction of heterologous protein expression, the growth of the cultures is slowed down due to the energy consumption for the expression of the corresponding protein (Mahalik et al., 2014). Based on the macroscopic appearance, all biofilms showed a homogeneously grown biomass after the initiation and expression phase of the enzyme of interest (Figure 3a). However, slight differences between various cultures and also fluctuations inside the flow cell were observed due to naturally occurring changes in biomass density within the flow channel. Moreover, a closer look revealed the expected heterogeneous structure of the biofilms independently which enzyme was expressed. The microscopic images also showed that the biofilms were riddled with micropores due to the flow of the medium (Figures 3b and S5).

For a closer insight into the biofilm formation, an *E. coli* biofilm expressing the red fluorescent protein variant (mRFP1) was cultivated in the microchannel to enable a more detailed examination of the biofilm structure by fluorescence microscopy (Figure 3c). The combination of fluorescence and DIC microscopy images, clearly indicated that in the biofilm matrix the fluorescent cells are surrounded by EPS, which can be seen as white colored structures in the merged images (Figure 3c, EPS + cells) and was confirmed by fluorescent counterstaining of the EPS using the standard dye CV (Stiefel et al., 2016) (Figure S6) and electron microscopy (Figure S7). Most of the biofilm can be removed by flushing the cultivation channel with air. The emptied channels then still contain a thin layer of biofilm adhering to the surface. Here, the fluorescence images clearly showed that this surface biofilm consists of cell aggregates separated from each other by empty spaces (see arrows in the insets of Figure 3c). This finding suggests that under these conditions the cells adhere less well to the PDMS surface without the biofilm matrix and the abundant EPS therein.

3.3 | Biocatalysis with productive biofilms

With the help of the above-described fluidic platform, the course of the enzymatic reactions within the biofilms was to be analyzed by sampling at different locations along the bioreactor flow channel. To allow a spatially resolved analysis of the biocatalytic activity of the biofilms, six sampling positions were defined, evenly distributed along the reactor channel (Figure 4a). In a representative experiment, after inoculation of the reactor channel, the biofilm was allowed to grow for 40 h in a continuous flow of LB medium before the expression of the recombinant enzyme was induced by addition of 1 mM IPTG. Following to further 20 h of cultivation, the channel was then perfused with a substrate solution (typically 5 mM substrate in LB medium). After an equilibration time of twice the residence time of the channel (about 30 min), samples were taken at the designated sites by the automated sampling robot. The collected samples were analyzed using established HPLC methods to quantify the amounts of product formed and remaining educt. To quantify the reproducibility of the biofilm cultivation, the expression of the enzymes and the location-dependent productivity of the biofilm, samples for the analysis of the reaction progress were taken from two independent chips, both of which were sampled twice in succession at the indicated sampling points. As shown in Figures 4b,c and 5a, all three biocatalytic systems exhibited, as expected, the decrease of educt and increase of products as the reaction path in the flow channel progressed.

The microreactors containing LbADH biofilms showed that about 50% of substrate **1** was converted into the corresponding products. Thus, about 29% of hydroxyketone **2a**, 16% of hydroxyketone **2b** and 7% of diol **3a** were formed at the rear end of the channel (Figure 4b). The diastereomeric ratio of **2a**:**2b** was found to be about 64:36, which corresponds well to the previously described values obtained in conventional reactions using the isolated enzyme (Peschke, Skoupi, et al., 2017; Skoupi et al., 2015). We also found that the cultivation of the catalytically active biofilms in two independent bioreactors led to comparable conversions with a *SD* of ±5% maximum. This result is remarkable and underlines the fact that the microfluidic system creates highly reproducible conditions with which even the highly complex biofilms can be handled reliably and controllably.

Since the prochiral C_S-symmetrical NDK **1** can as well be reduced by the *(S)*-selective ketoreductase Gre2p (Skoupi et al., 2015), similar experiments were then carried out with recombinant biofilms expressing the Gre2p enzyme. It is shown in Figure 4c, that the conversion rate was somewhat lower than that of LbADH, thus leading to an about 30% conversion of substrate **1** to yield exclusively hydroxy ketone **2c** as the sole product. The slightly lower activity of the Gre2p compared to the LbADH is in agreement with previously published data (13.7 $\mu mol_{substrate} \cdot min^{-1} \cdot mg_{protein}{}^{-1}$ (Peschke et al., 2018) or 5.9 $\mu mol_{substrate} \cdot min^{-1} \cdot mg_{protein}{}^{-1}$ (Bitterwolf et al., 2019) for LbADH or Gre2p, respectively). This study on the integration of ketoreductase Gre2p thus expands the range of productive biofilms available.

To extend the application range of the developed microfluidic platform, we also investigated, for the first time, the possibility to perform a decarboxylation reaction with an EsPAD biofilm. This study was of particular interest due to the production of carbon dioxide as a by-product of the reaction, which can lead to the formation of carbon dioxide gas bubbles inside the bioreactor. This in turn can lead to high local shear force peaks, which can cause damage to the biofilm (Sharma et al., 2005). However, our experiment

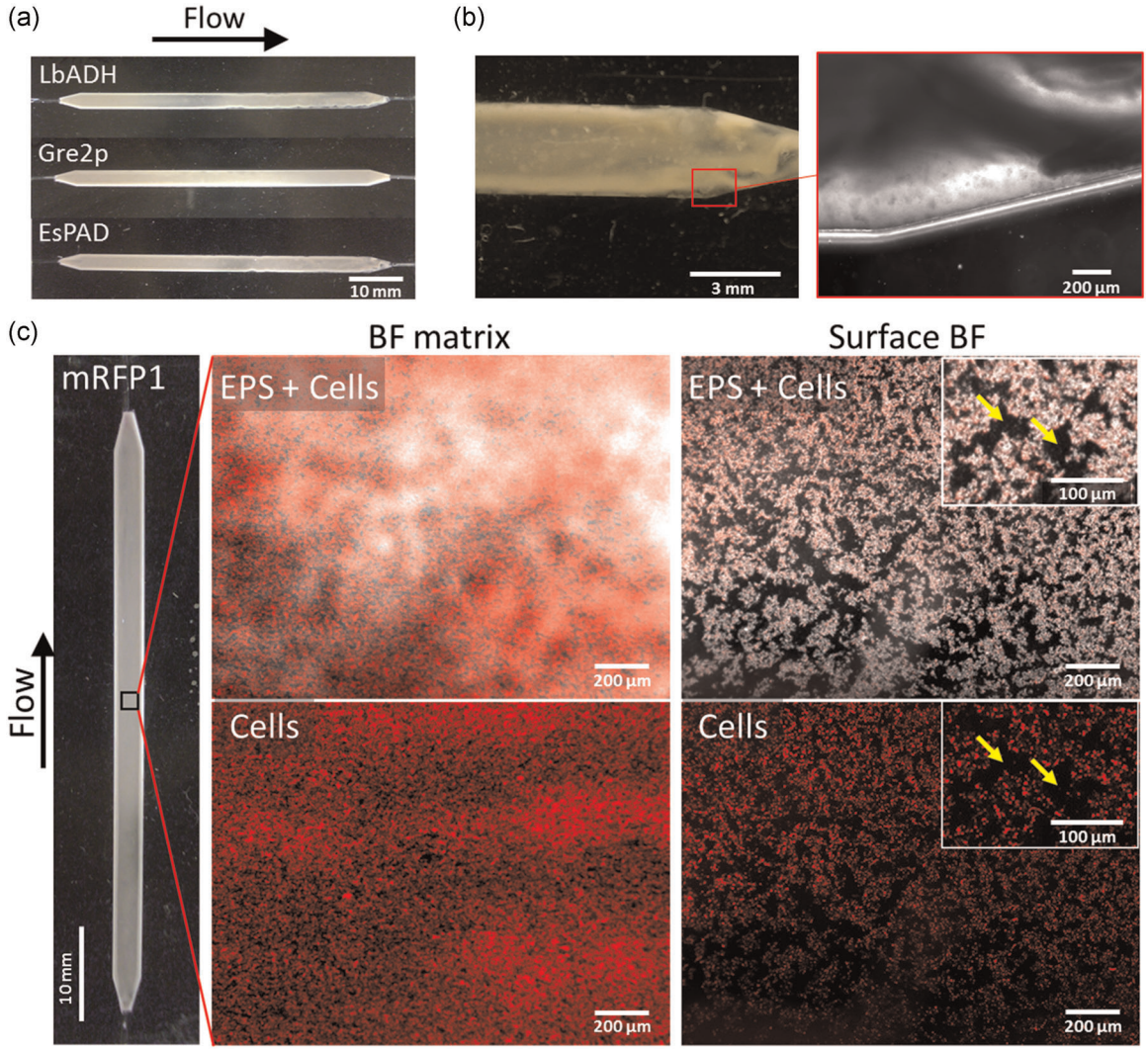

FIGURE 3 Microfluidic cultivation of recombinant enzyme-expressing biofilms. (a) *Escherichia coli* biofilms transformed with plasmids for the three enzymes, LbADH, Gre2p, and EsPAD. (b) The resulting biofilms have a cream-colored appearance after the expression phase and micrographs reveal typical heterogenic biomass structures. (c) *E. coli* biofilms encoding the red fluorescent protein variant, mRFP1. Microscopy images of the biofilm matrix (BF matrix) inside the chip reveal a mixture of cells (red) embedded in the EPS (white). Removal of the biofilm matrix from the channel by flushing with air results in a layer of surface-attached biofilm remaining in the channel (surface BF). The arrows in the inset images show empty spaces between cell aggregates of the surface BF. EPS, extracellular polymeric substances [Color figure can be viewed at wileyonlinelibrary.com]

with the EsPAD biofilm (carried out as described above) did not show any evidence of disturbance of the biofilm through the production of CO_2. Instead, the results showed that at a flow rate of 6 µl/min at the end of the bioreactor an almost complete substrate conversion of ≥99% was achieved (Figure 5a). The absence of interfering CO_2 bubbles indicates that rapid equilibration of the gas phases inside and outside the PDMS bioreactor occurs, which is enabled by gas diffusion through the PDMS based on partial pressure gradients (Fick's law) combined with the high gas permeability of PDMS (Dhingra & Marand, 1998; Merkel et al., 2000).

It is worth mentioning that in none of the investigated catalytically active biofilms a linear progression of substrate turnover and product formation along the bioreactor was observed. Instead, independent from the expressed enzyme, the conversion rate attenuated constantly over the length of the bioreactor (Figures 4 and 5). To further investigate this phenomenon, we took advantage of our microfluidic system and performed an in-depth analysis of the EsPAD biofilm in terms of its growth behavior and expression of the enzyme at different locations in the reactor channel. To this end, an overgrown channel was cut into five parts, and the biomass contained therein was extracted and quantified via OD measurement at 600 nm. Although the comparability of OD values over time in biofilm experiments is well known (Bakke et al., 2001), we experimentally confirmed that any EPS aggregates do not significantly affect OD measurements when we correlate these data with the protein content detectable in SDS-PAGE analyses of the segmented biofilms. As shown in Figure S8, we found no relevant differences in the protein content of the different segmented parts of the productive biofilms when the same OD was loaded into

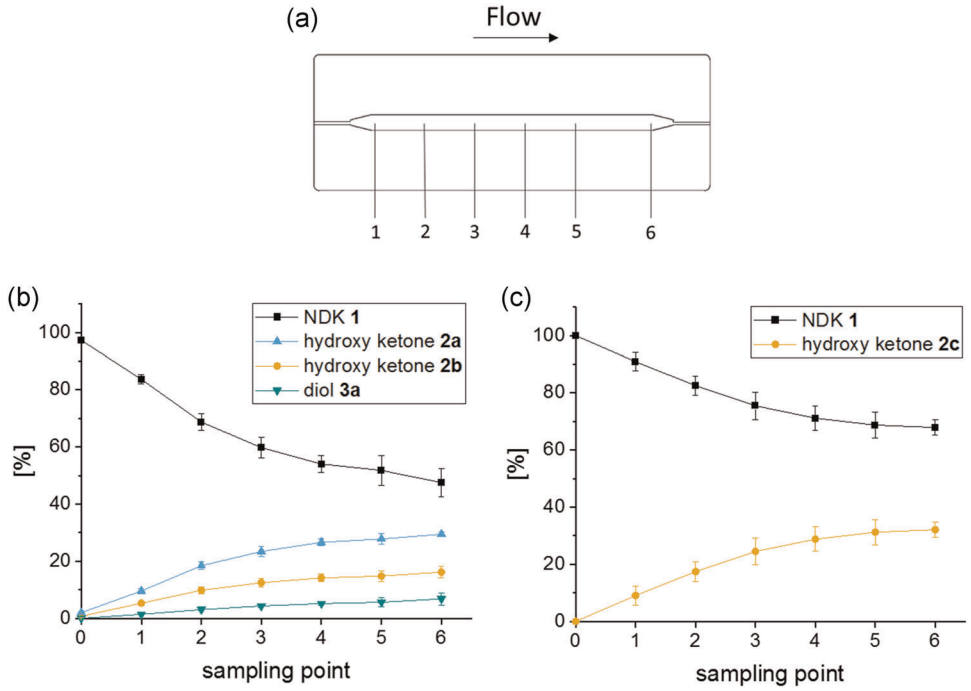

FIGURE 4 Spatially resolved conversion of prochiral NDK **1** with microfluidically cultured biocatalytically active biofilms. (a) Scheme of the sampling positions distributed on the microfluidic bioreactor channel. The arrow indicates the flow direction. (b) Conversion of the NDK **1** into the corresponding hydroxy ketones **2a**/**2b** and diol **3** products using LbADH. (c) Conversion of NDK **1** into hydroxy ketone **2c** using Gre2p. Initial substrate concentration of 5 mM and a flow rate of 6 µl/min were used. Samples were drawn machine-assisted with the same flow rate and quantified by HPLC. Sampling point 0 represents the substrate solution reservoir of the cultivation setup. The error bars represent the *SD* of two independent chips, each of which were sampled twice sequentially at the indicated sampling points. NDK, nitro-diketone substrate [Color figure can be viewed at wileyonlinelibrary.com]

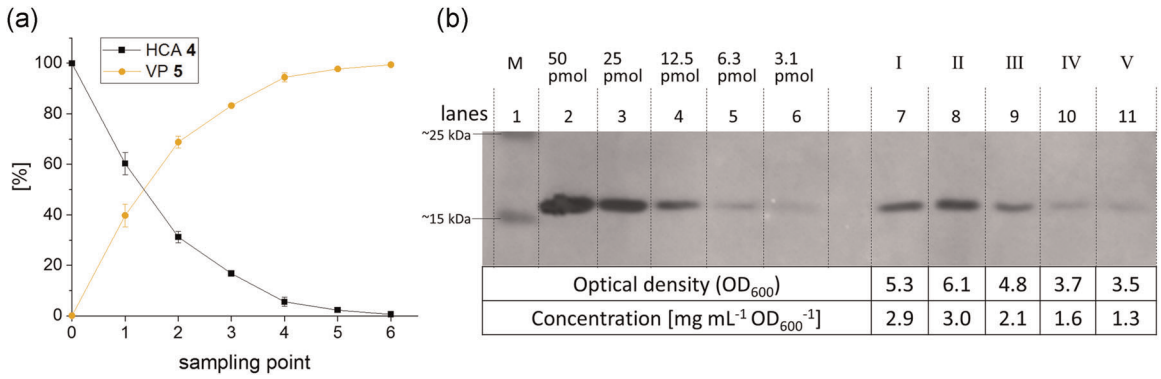

FIGURE 5 Spatially resolved analysis of an EsPAD-expressing biofilm. (a) Conversion of HCA **4** to VP **5**. EsPAD was expressed in fluidically cultivated *Escherichia coli* biofilms employing an initial substrate concentration of 5 mM and a flow rate of 6 µl/min. Samples were drawn machine-assisted with the same flow rate and quantified by HPLC. Sampling point 0 represents the substrate solution reservoir of the cultivation setups, while the other sampling points are distributed over the channel as shown in Figure 4a. The error bars represent the *SD* of two independent chips, each of which was sampled twice sequentially at the indicated sampling points. (b) Quantification of the EsPAD expression within a biofilm cultured in the microfluidic reactor. The cultivation flow cell was cut into five equal parts (I–V, with I at the beginning and V at the end of the flow cell), and the total biomass and the amount of expressed EsPAD in each part were determined photometrically and by western blot analysis, respectively. For a detailed description, see Figure S9. The shown cutout of the western blot contains the protein marker "PageRuler Prestained Protein Ladder" (M, lane 1), EsPAD calibration samples in variable amounts from 50 to 3.1 pmol (lanes 2–6) and biofilm samples obtained from parts I–V (lanes 7–11) of the flow cell. The table at the bottom shows the calculated enzyme concentration normalized to the biomass (optical density) of the biofilm obtained from the respective sections. Note that biomass and EsPAD expression decrease at the end of the flow cell. HCA, 4-hydroxycinnamic acid; VP, 4-vinylphenol [Color figure can be viewed at wileyonlinelibrary.com]

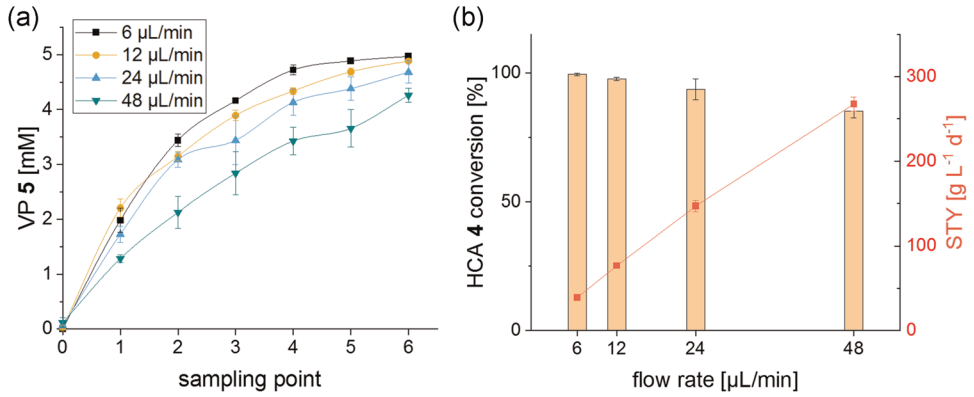

FIGURE 6 Optimization of the EsPAD biofilm reactor, using the conversion of HCA **4** to VP **5**. (a) Flow rate dependency of product formation determined at variable sampling points. Sampling point 0 is the starting concentration in the substrate solution reservoir. Quantification was achieved via HPLC and error bars represent the *SD* of two independent chip experiments, both sampled twice in a row at the specified sampling points. (b) Flow rate dependency of total conversion of **4** (bars) and corresponding STY (red line), as determined from the amounts of converted substrate measured at sampling point 6. All reactions were performed at a substrate concentration of 5 mM of HCA **4**. HCA, 4-hydroxycinnamic acid; STY, space-time yields; VP, 4-vinylphenol [Color figure can be viewed at wileyonlinelibrary.com]

individual gel lanes. Therefore, the enzyme content could be directly correlated with the OD of the biofilm.

The amount of recombinant EsPAD enzyme in the five parts was quantified by western blot analysis (Figures 5b and S9). The results indicate that the biomass is reduced by about 34% (OD_{inlet}: 5.3; OD_{outlet}: 3.5) and the amount of expressed EsPAD is decreased by 43% (normalized to the OD) at the end of the channel. These results suggest that due to the lower biomass as well as the lower enzyme concentration along the bioreactor flow path the reaction rate is reduced. The in-depth analysis of biofilm growth was also conducted for the LbADH and the Gre2p biofilms and a comparable behavior could be observed (Figure S10). It is worth mentioning here that the enzyme concentration does not decrease proportionally to OD, indicating reduced enzyme expression at the end of the bioreactor, probably due to reduced availability of nutrients in the downstream regions of the reactor channel. Since enzyme expression occurs in a microfluidic setup with continuous delivery of the inducing reagent and thus the enzyme is produced continuously, enzyme stability should not be a limiting factor and thus not responsible for the observed decreasing gene expression within the flow reactor. It is also noteworthy that the comparison of OD of wild type (*E. coli* BL21) biofilms with the biofilms heterologously expressing additional enzymes revealed that the recombinant biofilms produced significantly more biomass than the wild type (Figure S8). This may be due to the influence of antibiotics in the medium on biofilm formation and density. Also, it is known that the presence of a plasmid itself can influence biofilm formation (Teodosio et al., 2012).

Since the EsPAD biofilm was outstanding in terms of both stability and productivity, we chose this system as a model for further optimization of the system. To this end, we investigated the flow rate-dependency of the biofilm-catalyzed conversion of HCA **4** to VP **5** (Figure 6). We observed that gradual increase in the flow rate from 6–48 µl/min led to formation of less product, as determined at the various sampling points (Figure 6a). Specifically, the conversion at 6 µl/min with >99% was decreased stepwise to 98% (12 µl/min), 94% (24 µl/min) and 85% at a flow rate of 48 µl/min. In fact, this result was in line with expectations, since increasing the flow rate leads to a shorter residence time of the educts in the catalyst bed and thus to less product formation. However, the available STY, which provide a measure of the volumetric productivity of the reactor, increased with increasing flow rates (Figure 6b). As such, STY were found to increase from 39 $g \cdot l^{-1} \cdot d^{-1}$ (6 µl/min) over 77 $g \cdot l^{-1} \cdot d^{-1}$ (12 µl/min) and 147 $g \cdot l^{-1} \cdot d^{-1}$ (24 µl/min) up to 268 $g \cdot l^{-1} \cdot d^{-1}$ at a flow rate of 48 µl/min. One effect on this improvement in productivity could be the increasing shear forces due to the higher flow rates, leading to an adapted and thus denser biofilm. This is due to hydrodynamics playing a major role in biofilm formation, as previously shown in an aqueous-air segmented flow system (Karande et al., 2014). These results show very clearly how the productivity of the system can be significantly improved by optimizing the flow rate. Compared to established biofilm production reactors, such as the fixed-bed reactor, in which high shear forces can lead to biofilm detachment (Muffler et al., 2014), our microfluidic system provides stable conditions mainly in terms of flow properties by maintaining a low and controllable Reynolds number, resulting in laminar flow and low shear stresses. Conventional upscaling by increasing the size of the reactor is not possible in microfluidics, as this would completely change the hydrodynamic properties. Instead, upscaling can be easily achieved by running many of the chips in parallel (so-called "numbering up").

4 | CONCLUSION

In summary, we have reported here the application of a machine-based microfluidic biofilm cultivation and analysis platform for studying the performance of biocatalytically active biofilms. By using robotic sampling, we succeeded in spatially resolving the productivity

of three reactors containing biocatalytically active biofilms that inducibly overexpress a recombinant enzyme. The excellent reproducibility of the cultivation and analysis method observed in all three systems underlines the usefulness of the new technical platform for the investigation of biofilms. In addition, we demonstrated that our analytical platform also opens up new opportunities to perform in-depth spatially resolved studies on the biomass growth in a reactor channel and its biochemical productivity. In addition to this detailed biochemical characterization, the platform also offers broad capabilities for the morphological study of living biofilms. We believe that the studies shown here can also be performed on many other natural and artificial microbial communities to systematically investigate a wide range of process parameters in a highly parallel manner using miniaturized model systems, thus advancing the harnessing of biofilms for technical purposes.

ACKNOWLEDGEMENTS

This study was financially supported through the Helmholtz Association program "Materials Systems Engineering" under the topic "Adaptive and Bioinstructive Materials Systems". We thank Svenja Moench for the TEM analysis and Sandra Kröll and Sarah Bischof for experimental help. Open Access funding enabled and organized by Projekt DEAL.

CONFLICT OF INTERESTS

The authors declare that there is no conflict of interests.

AUTHOR CONTRIBUTIONS

Phillip Lemke performed the biofilm cultivation and biotransformation experiments and subsequent data analysis. Phillip Lemke and Ahmed E. Zoheir conducted the biofilm imaging and data analysis. Christof M. Niemeyer, Kersten S. Rabe, Ahmed E. Zoheir and Phillip Lemke designed the study and wrote the manuscript. Christof M. Niemeyer supervised the project. All authors discussed the results and approved the manuscript.

DATA AVAILABILITY STATEMENT

The data that support the findings of this study are available from the corresponding author upon reasonable request.

ORCID

Phillip Lemke http://orcid.org/0000-0002-0726-5023
Ahmed E. Zoheir http://orcid.org/0000-0001-5656-2932
Kersten S. Rabe http://orcid.org/0000-0001-7909-8191
Christof M. Niemeyer http://orcid.org/0000-0002-8837-081X

REFERENCES

Ahan, R. E., Saltepe, B., Apaydin, O., & Seker, U. O. S. (2019). Cellular biocatalysts using synthetic genetic circuits for prolonged and durable enzymatic activity. *ChemBioChem*, *20*(14), 1799–1809. https://doi.org/10.1002/cbic.201800767

Alves, P., Gomes, L. C., Rodriguez-Emmenegger, C., & Mergulhao, F. J. (2020). Efficacy of a poly(MeOEGMA) brush on the prevention of Escherichia coli biofilm formation and susceptibility. *Antibiotics*, *9*(5), 216. https://doi.org/10.3390/antibiotics9050216

Bakke, R., Kommedal, R., & Kalvenes, S. (2001). Quantification of biofilm accumulation by an optical approach. *Journal of Microbiological Methods*, *44*(1), 13–26. https://doi.org/10.1016/S0167-7012(00)00236-0

Bitterwolf, P., Gallus, S., Peschke, T., Mittmann, E., Oelschlaeger, C., Willenbacher, N., Rabe, K. S., & Niemeyer, C. M. (2019). Valency engineering of monomeric enzymes for self-assembling biocatalytic hydrogels. *Chemical Science*, *10*(42), 9752–9757. https://doi.org/10.1039/c9sc04074a

Blank, L. M., Ebert, B. E., Buhler, B., & Schmid, A. (2008). Metabolic capacity estimation of Escherichia coli as a platform for redox biocatalysis: constraint-based modeling and experimental verification. *Biotechnology and Bioengineering*, *100*(6), 1050–1065. https://doi.org/10.1002/bit.21837

Cuny, L., Pfaff, D., Luther, J., Ranzinger, F., Ödman, P., Gescher, J., Guthausen, G., Horn, H., & Hille-Reichel, A. (2019). Evaluation of productive biofilms for continuous lactic acid production. *Biotechnol Bioengin*, *116*(10), 2687–2697. https://doi.org/10.1002/bit.27080

Dhingra, S. S., & Marand, E. (1998). Mixed gas transport study through polymeric membranes. *Journal of Membrane Science*, *141*(1), 45–63. https://doi.org/10.1016/S0376-7388(97)00285-8

Drescher, K., Shen, Y., Bassler, B. L., & Stone, H. A. (2013). Biofilm streamers cause catastrophic disruption of flow with consequences for environmental and medical systems. *Proceedings of the National Academy of Sciences of the United States of America*, *110*(11), 4345–4350. https://doi.org/10.1073/pnas.1300321110

Flemming, H. C., Wingender, J., Szewzyk, U., Steinberg, P., Rice, S. A., & Kjelleberg, S. (2016). Biofilms: An emergent form of bacterial life. *Nature Reviews Microbiology*, *14*(9), 563–575. https://doi.org/10.1038/nrmicro.2016.94

Halan, B., Buehler, K., & Schmid, A. (2012). Biofilms as living catalysts in continuous chemical syntheses. *Trends in Biotechnology*, *30*(9), 453–465. https://doi.org/10.1016/j.tibtech.2012.05.003

Hall-Stoodley, L., Costerton, J. W., & Stoodley, P. (2004). Bacterial biofilms: From the natural environment to infectious diseases. *Nature Reviews Microbiology*, *2*(2), 95–108. https://doi.org/10.1038/nrmicro821

Hansen, S. H., Kabbeck, T., Radtke, C. P., Krause, S., Krolitzki, E., Peschke, T., Gasmi, J., Rabe, K. S., Wagner, M., Horn, H., Hubbuch, J., Gescher, J., & Niemeyer, C. M. (2019). Machine-assisted cultivation and analysis of biofilms. *Scientific Reports*, *9*(1), 8933. https://doi.org/10.1038/s41598-019-45414-6

Hoschek, A., Heuschkel, I., Schmid, A., Bühler, B., Karande, R., & Bühler, K. (2019). Mixed-species biofilms for high-cell-density application of *Synechocystis* sp. PCC 6803 in capillary reactors for continuous cyclohexane oxidation to cyclohexanol. *Bioresource Technol*, *282*, 171–178. https://doi.org/10.1016/j.biortech.2019.02.093

Karande, R., Halan, B., Schmid, A., & Buehler, K. (2014). Segmented flow is controlling growth of catalytic biofilms in continuous multiphase microreactors. *Biotechnology and Bioengineering*, *111*(9), 1831–1840. https://doi.org/10.1002/bit.25256

Karande, R., Schmid, A., & Buehler, K. (2016). Applications of multiphasic microreactors for biocatalytic reactions. *Organic Process Research & Development*, *20*(2), 361–370. https://doi.org/10.1021/acs.oprd.5b00352

Mahalik, S., Sharma, A. K., & Mukherjee, K. J. (2014). Genome engineering for improved recombinant protein expression in *Escherichia coli*. *Microbial Cell Factories*, *13*, 177. https://doi.org/10.1186/s12934-014-0177-1

Merkel, T. C., Bondar, V. I., Nagai, K., Freeman, B. D., & Pinnau, I. (2000). Gas sorption, diffusion, and permeation in poly(dimethylsiloxane). *Journal of Polymer Science Part B: Polymer Physics*, *38*(3), 415–434. https://doi.org/10.1002/(Sici)1099-0488(20000201)38:33.0.Co;2-Z

Mittmann, E., Gallus, S., Bitterwolf, P., Oelschlaeger, C., Willenbacher, N., Niemeyer, C. M., & Rabe, K. S. (2019). A phenolic acid

decarboxylase-based all-enzyme hydrogel for flow reactor technology, *Micromachines*. 10(12), 795. https://doi.org/10.3390/mi10120795

Mittmann, E., Hu, Y., Peschke, T., Rabe, K. S., Niemeyer, C. M., & Bräse, S. (2019). Chemoenzymatic synthesis of O-containing heterocycles from α-diazo esters. *ChemCatChem*, *11*(22), 5519–5523. https://doi.org/10.1002/cctc.201901602

Muffler, K., Lakatos, M., Schlegel, C., Strieth, D., Kuhne, S., & Ulber, R. (2014). Application of biofilm bioreactors in white biotechnology. *Productive Biofilms*, *146*, 123–161. https://doi.org/10.1007/10_2013_267

Muffler, K., & Ulber, R. (2014). *Productive biofilms* (Vol. 146). Springer.

Nussbaumer, M. G., Nguyen, P. Q., Tay, P. K. R., Naydich, A., Hysi, E., Botyanszki, Z., & Joshi, N. S. (2017). Bootstrapped Biocatalysis: Biofilm-Derived Materials as Reversibly Functionalizable Multienzyme Surfaces. *ChemCatChem*, *9*(23), 4328–4333. https://doi.org/10.1002/cctc.201701221

Peng, M., Mittmann, E., Wenger, L., Hubbuch, J., Engqvist, M. K. M., Niemeyer, C. M., & Rabe, K. S. (2019). 3D-printed phenacrylate decarboxylase flow reactors for the chemoenzymatic synthesis of 4-hydroxystilbene. *Chemistry*, *25*, 15998–16001. https://doi.org/10.1002/chem.201904206

Peschke, T., Bitterwolf, P., Gallus, S., Hu, Y., Oelschlaeger, C., Willenbacher, N., Rabe, K. S., & Niemeyer, C. M. (2018). Self-assembling all-enzyme hydrogels for flow biocatalysis. *Angewandte Chemie*, *57*(52), 17028–17032. https://doi.org/10.1002/anie.201810331

Peschke, T., Bitterwolf, P., Hansen, S., Gasmi, J., Rabe, K. S., & Niemeyer, C. M. (2019). Self-immobilizing biocatalysts maximize space–time yields in flow reactors. *Catalysts*, *9*(2), 164. https://doi.org/10.3390/catal9020164

Peschke, T., Rabe, K. S., & Niemeyer, C. M. (2017). Orthogonal surface tags for whole-cell biocatalysis. *Angewandte Chemie*, *56*(8), 2183–2186. https://doi.org/10.1002/anie.201609590

Peschke, T., Skoupi, M., Burgahn, T., Gallus, S., Ahmed, I., Rabe, K. S., & Niemeyer, C. M. (2017). Self-immobilizing fusion enzymes for compartmentalized biocatalysis. *ACS Catalysis*, *7*(11), 7866–7872. https://doi.org/10.1021/acscatal.7b02230

Schindelin, J., Arganda-Carreras, I., Frise, E., Kaynig, V., Longair, M., Pietzsch, T., Preibisch, S., Rueden, C., Saalfeld, S., Schmid, B., Tinevez, J. Y., White, D. J., Hartenstein, V., Eliceiri, K., Tomancak, P., & Cardona, A. (2012). Fiji: An open-source platform for biological-image analysis. *Nature Methods*, *9*(7), 676–682. https://doi.org/10.1038/nmeth.2019

Schmutzler, K., Kupitz, K., Schmid, A., & Buehler, K. (2017). Hyperadherence of Pseudomonas taiwanensis VLB120ΔC increases productivity of (S)-styrene oxide formation. *Microbial Biotechnol*, *10*(4), 735–744. https://doi.org/10.1111/1751-7915.12378

Sharma, P. K., Gibcus, M. J., van der Mei, H. C., & Busscher, H. J. (2005). Influence of fluid shear and microbubbles on bacterial detachment from a surface. *Applied and Environmental Microbiology*, *71*(7), 3668–3673. https://doi.org/10.1128/AEM.71.7.3668-3673.2005

Skoupi, M., Vaxelaire, C., Strohmann, C., Christmann, M., & Niemeyer, C. M. (2015). Enantiogroup-differentiating biocatalytic reductions of prochiral c-symmetrical dicarbonyl compounds to meso compounds. *Chemistry*, *21*(24), 8701–8705. https://doi.org/10.1002/chem.201500741

Stiefel, P., Rosenberg, U., Schneider, J., Mauerhofer, S., Maniura-Weber, K., & Ren, Q. (2016). Is biofilm removal properly assessed? Comparison of different quantification methods in a 96-well plate system. *Applied Microbiology and Biotechnology*, *100*(9), 4135–4145. https://doi.org/10.1007/s00253-016-7396-9

Teodosio, J. S., Simoes, M., & Mergulhao, F. J. (2012). The influence of nonconjugative *Escherichia coli* plasmids on biofilm formation and resistance. *Journal of Applied Microbiology*, *113*(2), 373–382. https://doi.org/10.1111/j.1365-2672.2012.05332

Toepke, M. W., & Beebe, D. J. (2006). PDMS absorption of small molecules and consequences in microfluidic applications. *Lab on a Chip*, *6*(12), 1484–1486. https://doi.org/10.1039/b612140c

Verstraete, W. (2015). The manufacturing microbe. *Microbial Biotechnology*, *8*(1), 36–37. https://doi.org/10.1111/1751-7915.12183

Willrodt, C., Halan, B., Karthaus, L., Rehdorf, J., Julsing, M. K., Buehler, K., & Schmid, A. (2017). Continuous multistep synthesis of perillic acid from limonene by catalytic biofilms under segmented flow. *Biotechnology and Bioengineering*, *114*(2), 281–290. https://doi.org/10.1002/bit.26071

SUPPORTING INFORMATION

Additional Supporting Information may be found online in the supporting information tab for this article.

How to cite this article: Lemke, P., Zoheir, A. E., Rabe, K. S., & Niemeyer, C. M. (2021). Microfluidic cultivation and analysis of productive biofilms. *Biotechnology and Bioengineering*, 1–11. https://doi.org/10.1002/bit.27861